Intrinsic radiation resistance of mesenchymal cancer stem cells and implications for treatment response in a murine sarcoma model

Filippo Peder D'Andrea

This review has been accepted as a thesis together with three original papers by Aarhus University 18th of July 2011 and defended on 13th of December 2011

Tutor(s): Akmal Safwat, Michael R Horsman & Jens Overgaard

Official opponents: Dietmar Siemann, Hans Skougaard Poulsen & Marianne Nordsmark

Correspondence: Department of Experimental Clinical Oncology, Aarhus University Hospital, Nørrebrogade 44, bldg. 5, 8000 Aarhus C, Denmark

E-mail: filippo@oncology.dk

Dan Med J 2012;59(2):B4388

ORIGINAL MANUSCRIPTS

This review is based on the following original manuscripts.

1. D'Andrea FP, Horsman M, Kassem M, Overgaard J, Safwat A. Tumourigenicity and radiation resistance of mesenchymal stem cells. Acta Oncologica 2011. Available online, in press.
2. D'Andrea FP, Safwat A, Burns JS, Kassem M, Horsman M, Overgaard J. Tumour microenvironment and radiation response in sarcomas originating from tumourigenic human mesenchymal stem cell. Submitted to Int. Journal of Radiation Biology. Revised.
3. D'Andrea FP, Safwat A, Kassem M, Gautier L, Overgaard, J, Horsman M. Cancer stem cell overexpression of nicotinamide N-methyltransferase enhances cellular radiation resistance. Radiotherapy and Oncology 2011:99;373-378.

BACKGROUND

Tumour resistance to irradiation is the most challenging obstacle facing modern radiotherapy. Historically, cancer was viewed as a mass of rapidly proliferating cells, and therapeutics were designed to eliminate highly proliferative cells. Radiation resistance was believed to result from the intrinsic radiation resistance of tumour cells as well as from microenvironmental induced hypoxia resulting from inadequacies of the tumour's normal tissue derived vasculature's ability to supply oxygen.

Recent studies provide evidence for the role of stem cells in neoplastic transformation and tumour growth properties and link neoplastic growth with stem cell biology. Tumours are now believe to arise from tissue stem cells or their immediate progeny rather than from normal lineage committed cells with induced stem cell characteristics. The resistance of these cancer stem cells (CSC) to chemo and radiotherapy may therefore explain why such therapies often fail. Microenvironmental factors such as hypoxia may affect CSC resistance to treatment since these are now know to be maintained in vascular niches in the tumour with a defined microenvironment and that oxygen levels may promote expression of stem cell markers.

Based on this new knowledge it is argued that classical essential questions regarding tumour response to radiotherapy need to be readdressed and restudied at stem cell level in a suitable model. This work is dealing with questions regarding tumourigenicity and radiation resistance of stem cells; possible genetic key factors determining radiation resistance and the relationship between in-vitro radio-sensitivity of CSCs and the in-vivo microenvironmental factors known to affect the response to irradiation. This is being investigated in a novel and unique stem cell derived sarcoma model based on human bone marrow derived mesenchymal stem cell that spontaneously acquired the ability to form tumours in nude mice. Xenografts formed from subclones of this original cell line show behavioural differences that allow for comparisons to be made between cellular traits and in vivo microenvironmental characteristics and correlations to be drawn with response to therapy.

Ionizing radiation

The use of ionizing radiation as a treatment for cancer is a long established tradition. The technical concept of exposing the area to be treated to nuclear decay or an electrical generated beam is relatively simple. But ionizing radiation is damaging for both normal and malignant cells alike and side effects, such as telangiectasia [1], fibrosis [2], organ failure and patient death [3] has to be minimised. Modern radiotherapy application has, therefore, become rather sophisticated and oriented towards conforming the radiotherapy dose to the target area [4].

The radiation that passes through the treated cells will form free radicals, which will disrupt the bindings between DNA nucleotides and breaks the DNA strand. The radiation induced free radicals and ROS will react with DNA and protein in a desperate attempt to obtain the lacking electron for their unsaturated outer shell and thereby causing damage to the donor molecule. If the electron donor is a DNA bond then this will break leaving either a damage nucleotide or single strand break (SSB) in the chromosome [5].

Double strand break (DSB) can happen either due to multiple SSB at or near the same site or during synthesis of the new chromosome where the SSB will introduce a DSB when the replication

fork reaches the SSB [5]. In either case a broken chain of DNA is an alarming incidence for the cell, as DNA is the blueprint for the cell and any alteration to it can be detrimental for the cells survival and function. Therefore, damage response and repair mechanisms are activated to hinder the break becoming a catastrophic event for the cell.

Damage response

The chromosomes are continuously scanned for any signs of damage or mismatched base pairs by several proteins [6]. If a damaged site is detected, protein complexes are recruited and cellular processes activate damage repair mechanisms. The most common and fastest DNA damage sensor is activation of the ataxia telangiectasia mutated protein (ATM) [7]. ATM and the complex proteins that it interacts with seek out the damaged site and as a response to detected damage, start to phosphorylate downstream targets in a cascade. The histone H2AX at the damaged segment is phosphorylated and starts recruiting other proteins needed for DNA repair [8]. The next step is that both Mdm2 and p53 are regulated by the ATM [7] cascade and together determine whether the cell will undergo cell death via Bax induced apoptosis [9, 10]or cell cycle arrest through p21 inhibition of the G1-S cell cycle checkpoint [11]. The cells current place in the cell cycle also affects which pathway and proteins that respond to damage and when [12].

Damage repair

Damaged DNA activates several cellular responses competing over the cell's fate. Several genes become active, the cell cycle is slowed and cell division is prohibited until the cell's fate is decided. If the damage is within the cell's capacity to repair then the cell cycle will remain paused until the damage is repaired [12]. Damage to the DNA strand that is repaired correctly will have no further effect on the cell. However, the cell can tolerate error prone damage repair, although this could lead to incorporating of altered base pairs in the genome with point mutations as a result [13].

The cell has several ways of handling DNA damage repair depending on the type of damage inflicted. Damaged nucleotides are handled by either base excision repair (BER) and mismatch repair (MMR). While BER will only alter the base of the nucleotide, MMR on the other hand will remove a segment around the damaged nucleotide, where after polymerases fill out the missing segment [14].

SSB induced by ionising radiation is detected by the poly ATP ribose polymerases (PARP)[15], which continuously scans the chromosomes for damage. Upon finding a site of lesion, PARP will add a growing chain of ATP to the damaged site. This polymer chain of ATP ribose units (PAR) recruits several other DNA repair components to the damaged site [16]. If a SSB is not repaired before the synthesis of the new chromosome strand, the SSB can become a DSB, which is even more detrimental for the cell and will induce apoptosis if not repaired [12].

DSB is repaired with either homologue recombination (HR) [17] or non-homologue end-joining (NHEJ) [18]. The proteins that attach to the breakpoint promote either HR when the cell is in the S or G2 phase or NHEJ if the break is detected in the G1 phase. The need for a homologue segment of DNA to the site of breakage restricts HR to S and G2 phases where the chromosome has been duplicated [12]. NHEJ can occur in all phases of the cell cycle and while it is fast it is not as accurate as HR, since the repairs by NHEJ induce small deletions in DNA strand at the joining site. Although NHEJ makes deletion mutations, the fast process ensures that the cell may survive as the damage is repaired before a cell cycle check point that could have initiated apoptosis.

Apoptosis

If the cell is beyond salvage, due to too much DNA damage, then the apoptotic pathway is activated. ATM, ATR and other damage signal proteins will phosphorylate p53 making it more stabile and thereby increasing its activity [19, 20]. P53 enter the nucleolus where it functions as a transcription factor and increases the expression of several genes, including BAX [9], whose translated protein Bax will signal to the mitochondria for activation of the apoptotic pathway [10]. The mitochondria will release cytochrome C, which will activate a caspase cascade that will break down the cellular structure and the cell will undergo programmed cell death and fragmentation into apoptotic bodies.

Under normal circumstances the Mdm2 protein is a negative regulator of p53 activity as it retains p53 in the cytosol. But the MDM2 gene responds to increased p53 stability by increasing transcription of Mdm2 [21] in an attempt to retain the normal balance. Other proteins affect the p53 balance, such as the ARF protein, from the CDKN2A gene [22], which affects the efficiency of Mdm2 blockage of p53 activity as ARF inhibits the Mdm2 retention of p53 in the cytosol [23], allowing p53 to enter the nucleolus.

Other pathways, such as PARP activity, also affect the induction of necrosis and apoptosis [24]. While prolonging the PAR chain, PARP activity consumes ATP and NAD^+ [25]. If there are many sites of damage then the PARP polymerisation will deplete the cellular levels of ATP and NAD^+ and depletion of either will signal the mitochondria for induction of apoptosis [26]. There is a cellular balanced response to overpolymerisation by PARP as caspases can cleave PARP and thereby regulate the degree of polymerisation [27]. To a highly damaged cell, it will not be cost efficient to repair the damage and therefore a system such as the PAR elongation will assess the damage and can promote apoptosis when crossing a critical limit.

Stem cells

Stem cells are the foundation of all cells and organs in humans and all other higher organisms. The first cells of a new individual are totipotent stem cells that have within them the capability to differentiate into all cell types. Different influences, either from the location in the blastocyst, the organ wherein it resides or from extracellular chemical signals sends the stem cell on a defined route to final differentiation. The road from totipotent stem cell to final differentiated cell involves many stops on the way, with intermediate stem cells having less potential for differentiation and a defined roadmap telling which branches of differentiation is still accessible.

To insure that both differentiated cells and potent stem cell are present then cell division does not give rise to two equal daughter cells. Instead the stem cell divides asymmetrically into a daughter cell primed for differentiation and a stem cell that is similar to the original stem cells. This process ensures the preservation of a stem cell pool and that there is both continuity and a growing cellular mass that form organs though differentiation. The self renewed stem cell can continuously give rise to new differentiated cells to take over for the old and dying cells [28]

After many cycles of cell division one stem cell would have given rise to a horde of differentiated cells. Whereas the final differentiated cell lives for a relatively short time, only to enter into se-

nescence and subsequent programmed cell death then stem cells are characterised by their ability to live forever through evasion of apoptosis and senescence. This is mainly accomplished by the activity of TERT that ensures the continued presence of telomeres at the chromosomal ends in Stem cells [29].
The older and further away from the original embryonic totipotent stem cell, the less potent the stem cells are. Adult stem cells, found throughout the human body, are normally only capable of differentiating into a few cell types, as seen with adult mesenchymal stem cells, that normally only can give rise to osteoblasts, myocytes, adipocytes and chondrocytes [30]. Stem cells also migrate to a site in the host where they are needed and initiate healing of wounded tissue [31].

Cancer stem cells

At the core of cancer stem cells theory lays the concept of differentiation gone wrong. The stem cell has taken a wrong turn and is now out of bounds. It is easy to envision an alteration in adult stem cells' self-regulation that could give rise to a tumourigenic phenotype with enhanced proliferation and heterogenic cell progeny. This is often due to one or more genetic alteration that directly or in concert with other factors promotes a cancerous phenotype over a normal stem cell phenotype. The most classical genetic alteration is found in genes that regulate the cell cycle, such as RB and p21 or respond to DNA or cellular damage, such as p53 and Bax [32]. Also alterations with regard to longevity as with increased TERT activity or alternative lengthening of telomeres are commonly seen.
The literature operates with several names for related cell types involved in tumourigenicity; Tumour instigating cell, stem cell like tumour cells, clonogenic cells, transient amplifying cells, progenitor cells and cancer stem cells. All these terms are not necessarily describing the same cell type. While cancer stem cells may give rise to the tumour, the main tumour burden will normally consist of final differentiated tumour cells, progenitor cells and transient amplifying cells. Like with normal stem cells, cancer stem cells may differentiate into less potent progenitor cells and thereby give rise to tumour heterogeneity [33].
Several assays are used to isolate, purify and enrich the cancer stem cells from actual tumours and xenografts, based on cellular markers such as CD133+ for glioma [34], ovarian cancer [35] and sarcomas [36, 37] and CD44+CD24- for breast cancer stem cells [38]. However, these markers are not exclusively expressed on all CSC as some studies have shown that CD133+ cells were not able to generate tumours when transplanted [39]. Moreover, CD133 expression was seemingly lost when the cancer stem cells were kept in culture for prolonged periods [40]. The presence of CD44+CD24- cancer stem cells in tumours correlates with poor prognosis [41] and metastatic spread in breast cancer patients [42]. Patients with CD133 positive tumours had poor chance for progress free survival and low overall survival [43].
Cancer stem cells seem to share similar traits with normal stem cells, as both are considered immortal, capable of giving rise to differentiated progenies [44], as well as have self- renewing and asymmetric cell division [45]. Moreover, CSC are implicated in metastasis with mechanisms that mirror the cellular migration seen with stem cells [42]. Both CSC and stem cells can influence and are influenced by their surroundings and can initiate angiogenesis [46]. But a major difference between CSC and normal stem cells is CSC's self-sufficiency in growth signals and their insensitivity to anti-growth signals. Normal stem cells are under strict control by both their internal programming as well as the signals from the surroundings such as cell-cell interactions where as CSC seems unaffected by exterior anti-growth signals [45].

Tumours, microenvironment, hypoxia and radiation

The ionizing effect of radiation depends on the level of oxygen in and surrounding the target cells. Lack of oxygen leads to a hypoxic state which has a dire affect on radiation treatment as hypoxic cell [47] and tumours [48] are more resistant. The oxygen enhancement ratio is well described and manifests itself as less cell kill among hypoxic cells in in-vitro assays, and poorer tumour control after radiotherapy in in-vivo animal experiments as well as in patients with hypoxic tumours [49]. This is due to less free radicals and ROS generated after irradiation and therefore less DNA damage. There is indication that CSC may have lower levels of ROS [50], due to increased free radical scavenging, which may affect radiotherapy outcome.
The degree of hypoxia is defined by the efficiency of the vasculature and to some degree the distance of the tumour cells from the vasculature, as the cells will experience a falling gradient of oxygen the further away from the vasculature they are [51]. The more lack of oxygen the more hypoxic the cells become until no oxygen or nutrients reach the cells. Left without either the cells will eventually undergo necrosis. The most common cause for a hypoxic gradient is chaotic vasculature. The normal physiologic process of angiogenesis is not adhered to in a tumour and the new vasculature is often very poorly organised and blood flow through segments of it are sporadically blocked [52]. The areas without oxygen exist in a state of chronic hypoxia while the areas with temporarily blocked vasculature are in a state of acute hypoxia [51], and both types of hypoxia lead to decreased treatment success.
Sheltered within the chaotic vasculature cancer stem cells have niches to reside in; niches that protect them from radiation treatment [53, 54] and could induce stem cell like phenotypes in tumour cells [55]. The CD133+ tumour stem like cells in glioblastomas have been shown to obtain an enhanced radiation resistance when going from cell culture to xenografts, presumably due to microenvironmental influences on the cells capability to take up oxygen and their capability to handle and repair double strand breaks [56, 57].

Dedifferentiation and induced pluripotent stem cells

Though the CSC theory is gaining ground, the classical view of genetic alterations turning differentiated cells into tumour instigating cells still have some merit and is getting unexpected support from the field of stem cells research. The process from potent stem cell to defined terminal cell has been shown not to be unidirectional, as induced pluripotent stem cells have been made from several kinds of organisms and cell types [58, 59]. As few as four proteins are enough for a defined cell to reset to a stem cell or at least stem-like cell with the potential to differentiate to a new kind of cell type. This can either be due to a permanent integration of activated genes into the genome or as a transient induction by protein transfection into cells [60].
Of particular importance is the observation that several of the proteins that are involved in inducing pluripotent cells are also induced by hypoxia and may instigate the expression of stem cell proteins. HIF1α and HIF2α induce several of these proteins such as Notch, Sox2, Oct4, c-Myc and hTERT [61, 61, 62]. The four first mentioned are involved in induction of pluripotent stem cells [59] and c-Myc also is a known oncogene [63] and hTERT induces immortality in cells [64, 65]. This coupling between the microenvi-

ronment and tumour cell in the vascular niches may give rise to enhanced cancer cells which functions as CSC.

The telomerised mesenchymal cancer stem model

Adult mesenchymal stem cells in-vitro would normally undergo senescence and stop dividing after some population doublings. Through retroviral insertion of the human TERT subunit into mesenchymal stem cells Moustapha Kassem's research group circumvented the shortening of telomeres at the chromosomal ends [65], thereby granting the cells immortality. The model have not shown any sign of senescence and is still used for bone formation assays. The immortal cell line has been kept as three separate populations for a prolonged period, and handled nearly similarly; The only difference in handling of the cell lines were the split ratio when passaging the cell cultures [66]. The cell lines have been named after the spilt ratios and are thus called hMSC-TERT2 with a spilt ratio of 1 to 2, hMSC-TERT4 with a 1 o 4 ratio and hMSC-TERT20 which experienced the largest cellular stress by being spilt in a 1 to 20 ratio. All three cell lines were found to display mesenchymal stem cell markers and behaviour as all had the capability to generate mesoderm cell types when stimulated [67]. After continually passaging for 3 years, the immortalised hMSC-TERT20 cell line spontaneously generated sarcoma like tumours when implanted in nude NMRI mice [66]. Tumours that has been characterised as presumably Ewing's sarcoma like [68]. The TERT20 cell line has a deletion in the gene CDKN2A. Two different proteins are encoded by CDKN2A; p16 and ARF [22], both of which influence the cell cycle regulation as tumour suppressors. The protein p16 blocks CDK4, which is crucial for the progression through G_1 check point [22], and ARF inhibits the MDM2 protein blockage of p53 [23] which increased p21 expression and induces cell cycle arrest. As the TERT20 cell line has a deletion in the CDKN2A gene then the cell cycle is deregulated [66]. Also the gene DBC1, may influence the TERT20 phenotype, as it is a potential tumour suppressor gene and was found to be silenced by methylation in TERT20 [66] and other cancers [69]. The non-tumourogenic cell line, TERT4, shares the same deletion of the CDKN2A gene that hMSC-TERT20 does, but also has a k-Ras pointmutation [66].

The hMSC-TERT20 cell line was single cell cloned after it acquired tumourigenic capabilities [70] and the resulting collection of hMSC-TERT20 clones all shares the maternal cell line's overexpression of TERT, deletion of the CDKN2A gene and silencing of the DBC1 gene. They can all give rise to tumours in nude NMRI mice and have common cellular properties and surface markers[68], but the growth time of xenografts from injection to a final size of 1200mm^3 is different, as are some of the clones' requirements for serum [70]. These clones are ideal for close comparison into cellular causes for the displayed differences in phenotypes and treatment response.

In comparison, the hMSC-TERT2 sister cell line is still today in use as a bone formation model and has shown no signs of senescence nor malignant growth when implanted [71]. The close relationship between the three cell lines and the few but significant differences is a good starting point for several investigations into how cancer stem cells become what they are.

METHODS

Cell culturing

The cell lines used were originally established at The Molecular Endocrinology Unit at the University of Southern Denmark lead by Professor Moustapha Kassem. The founder cell line was purified from a bone marrow sample obtained from a healthy volunteer. Using a retroviral vector the human subunit TERT was permanently integrated under a constantly active promoter [65]. The immortalised cells, named hMSC-TERT were kept as three separate cell lines differing only in the spilt ratio when passaged. The number after the hMSC-TERT indicates whether the cell lines were spilt in a 1:2, 1:4 or 1:20 ratio when confluent. The hMSC-TERT20 was, after it acquired tumourigenic capabilities [66] single cell cloned into several cell lines [70].

In total, we received the cell lines MSC-TERT4 (TERT4), hMSC-TERT20 (TERT20) and cell line clones of the hMSC-TERT20 (BB3, BC8, BD6, BD11, CE8 and DB9). Initially, they were all amplified to ensure we had ample stock with the same passage number to conduct experiments. The cells were grown in MEM media (Gibco, Life Technology a/s) containing 10% Foetal Calf Serum (Life Technology a/s), 1% non-essential amino acid (Gibco, Life Technology a/s), 1% penicillin-streptomycin (Gibco, Invitrogen) and 1% sodium pyruvate (Gibco, Life Technology a/s), and incubated in 5% CO2 atmosphere and at 37°C in a incubator (Thermo Scientific, a/s Ninolab). When confluent the cells were split and seeded at $1*10^6$ cells in another T85 cell culture flask (Nunc, Denmark). The cell lines were, and still are, kept frozen at -140°C. Our laboratory routinely tests new cell lines for mycoplasma infection and none were found to be positive. The growth rate of all cell lines was also routinely assayed by seeding $1*10^5$ cells into several T25 flasks and then each day over a period of up to two weeks, three flasks were counted. The doubling time was calculated by the formula Td=(t2-t1)*(log(2)/(log(q2/q1)). Td being the doubling time in days, (t2-t1) is the difference in days between measurement 2 and 1, and (q2/q1) is the ratio of cells on day 2 and day 1.

Survival fraction assay and cell irradiation

The in-vitro clonogenic test for radiosensitivity is based on seeding cells, irradiating them, and then later counting the number of colonies. A dilution range is made by serial dilution from a known high starting concentration. The dilutions were done as 1:3 or 1:4 dilutions down to the lowest concentration of app. 200 cells per flask. Cells were seeded in T25 flasks (Nunc, Denmark) with 6 flasks per dose and single dose irradiation was performed 24 hours after seeding. The doses were 1, 2, 3, 4, 6 or 8Gy given at a dose rate of 0.58Gy/min using a 240 kV X-ray machine (Phillips, Holland). One week after irradiation, media was changed, and two weeks later the cells were fixed in methanol (VWR, Denmark) and stained with 50% toluidine blue (Ampliqon, Denmark). Colonies of at least 50 cells were counted and scored. The ratio between the numbers of colonies and the number of seeded cells was normalised with the Plating Efficiency (PE) to obtain the Survival Fraction estimate at the given dose. The formula is SF = colonies/(cells*PE), where PE is defined as the number of colonies divided by the number of seeded cells in the 0Gy (control) batch, and gives an estimate of the cells ability to survive the re-plating procedure. (PE=colonies/cells seeded at 0Gy). Each SF assay would result in one average PE estimate from the 0Gy flasks and one average SF value for each dose. All cell lines were tested in triplicates. Estimation of the alpha and beta values for the SF curves were done in Stata 10 (StataCorp, USA) by first transforming the SF values with the natural logarithm and then using non-linear regression with the formula Ln(SF)=(Dose*alpha)-(Dose*Dose*beta). The obtained alpha and beta values was sub-

sequently plotted in Sigmaplot (Systat Software Inc.) using the formula SF=exp((Dose*alpha)-(Dose*Dose*beta)).
To rule out the possibility that the plating efficiency might be the cause of a difference in the response to radiotherapy we conducted a feeder layer control experiment. Prior to performing the colony-forming unit assay described above cells were irradiated with 30Gy the day before and seeded into the assay culturing flask at a concentration of 10^4cells/cm^2. Twenty four hours after feeder layer seeding the normal colony forming unit assay was performed as described. As an estimation of a possible contribution of colonies from the irradiated feeder layer cells, 6 extra flasks with feeder layer were made which were not seeded with cells a second time. If there were more than 10 colonies in total in the feeder layer control flasks then the average colony number of the 6 feeder background flask was deducted from the colony count of each flask in the SF assay before calculating SF values. No feeder layer experiments were actually corrected in this way as there rarely was found any colonies in the 36 feeder background flasks counted in total (median is 0, mean is 0.44 [0.12:0.78], 95% confidence interval).
Using dilution rows may be a practical way of generating a series of concentrations but there are several pitfalls that have to be taken into considerations. First there is the starting concentration. As we use a Bürk counting chamber then there is some uncertainty in the estimation of the stock concentration simply due to human interference and this stock uncertainty will bleed down through the dilution row. Secondly there is the making of the specific concentrations used for each dose, as we pipet a volume from a defined sample over into a larger volume for a new concentration. The pipettes themselves have an uncertainty in the volume taken up and therefore in the amount of cells seeded in the next concentration. This will also affect the next concentration down the row. This volume uncertainty is most likely to give lower actual concentration in the lower concentration flask than calculated, as a small volume is taken into a larger volume and since the large volume is taken with a pipette having a higher uncertainty there is a bias towards larger volumes and lower concentrations. Also the correct concentration for the specific dose can be hard to estimate before-hand, therefore, half of the flasks to be used at each dose set was seeded with a normal cell concentration and the other half with a two to three times higher cell concentration. The high concentration colony counts were normalised to the normal concentration before having its SF value calculated. This leads to the problem with colony counting. The user is to assess when a colony is above the desired limit of 50 cells, which would indicate that the single cell that survived the radiation dose divided at least 5 times. As the counting is done under a stereomicroscope then the human bias again influences the outcome, however the chances of either over estimating or underestimating the cell number in a colony seems even, as long as the colonies are defined in size and clearly stained, although it should be kept in mind. Luckily modern technology can help those just beginning in the field. Flowcytometry machines are now capable of sorting a specific numbers of cells into separate test tube and therefore the dilution row bias can be countered. Also counting of colonies can be automated, as several software applications exist either commercial or non-profit which can assess the colonies that are above the defined limit for counting. Had we started the SF assays today at least the flowcytometry sorting would have been used instead of the manual generation of the dilution rows.
The cells used in the assay for radiation induced alteration in gene expression were handled as for the SF experiment, with some exception. Twenty-four hours before irradiation with 2Gy, $1*10^6$ cells were seeded in T25 flasks. Four hours after irradiation cells were collected and had total RNA purified with the miRNeasy Mini kit (Qiagen).

Exon expression arrays and data evaluation
Gene expression comparisons between samples were done in a similar way. Total RNA purified with the miRNeasy Mini kit (Qiagen) had the quality of the RNA assessed by the ratio between light absorption at 260nm and 280nm and had the quantity calculated directly from the absorption at 260nm. Care was taken to ensure that as little as possible contamination from the DNA in the Qiazol samples was transferred to the final purified RNA sample, as this would have a negative impact on the hybridisation to the array chips. Hybridisation on the Human Exon 1.0 ST array chip (Affymetrix, USA) and data extraction was done by the local supplier (Aros Applied Biosystem A/S, Denmark) but the resulting data files were handled in our own department. Normalisation was performed using Expression Console (Affymetrix, USA) with the RMA algorithm and restricting the dataset to the gene expression profile, using polished mean and sketch quartile. The choice of exon arrays over gene arrays was deliberate, as the gene arrays could have answered all our questions just as good at the exon arrays, but we had negotiated a price were the exon arrays was more accessible. Exon arrays main advantage is that all genes are represented by several probe sets matching each genes exon. The data from each probe set can either be handled individually as with the exon profile or combining all gene specific exon probe sets into a gene profile. Since the data volume from the gene profiles were more readily accessible, datapoints were combined into gene profile, leaving the exon profile of the chips for more detailed studies if needed. The resulting normalised data was linearised before gene expression alterations were found in a spread sheet set-up to look for an increase or decrease of more than 2-fold. Only differences between expression values above a background threshold of 40, estimated from plotting all data points and visually assessing the background level, were reported. The ratios between similar genes at different treatment times or form different cell lines is simply the mean for the values at time b divided by the value at time a. Therefore values higher than 1 would indicate an increased expression of the gene due to treatment or across cell lines.
Alternative normalisation algorithms were considered, but the RMA is efficient at the chip numbers analysed and is more conservative than the PLIER algorithm although small differences may go undetected (http://media.affymetrix.com/support/technical/technotes/plier_technote.pdf, white paper from Affymetrix). As there is no current perfect algorithm, the choice of RMA seemed best suited to a medium sized gene expression assay. Furthermore, only comparisons of results from the same chip batches were done to further reduce inter-chip difference. A chip batch is here defined as chips from the same production which were run at the same time and on the same machine.

Qualitative Reverse Transcription PCR
Further verification of the expressions levels was done by Real-Time PCR on RNA from the same samples used for the microarray experiment along with samples from the same experiments that were not previously analysed but were included in the original experiment as secondary samples. RNA samples were reversed transcribed and mixed with TaqMAN probes as per manufactures

description (Applied Biosystem, Europa) on an automatic pipetting robot (Biomek 3000, Beckman Coulter, Europa) and subsequent real-time PCR reaction was run and measured in a 7900HT Fast RealTime PCR machine (Applied Biosystem, Europa). As the TaqMAN probes were selected to cross over introns only spliced mRNA is detected, thereby removing any contribution from DNA that may not have been removed in the purification steps. We had originally selected the ACTB probe (Part nr. 4352935E) as reference gene but the deltaCT values were several orders away for the other samples so it gave high fluctuations in the normalised data for the other detectors. Instead the auxiliary reference probe, for the gene CHCHD1 (Hs00415054_m1) whose deltaCt values were in the same range as the other samples, was used. Comparisons between the means of the individual probes were done with Student's t-test using 0.05 as the level of significance. The ratios between similar probes at different treatment times or from different cell lines is simply the mean for the values at time b divided by the value at time a. Therefore, values higher than 1 would indicate an increased expression of the analysed probe.

Gene pathways

Gene expression arrays give a vast amount of data. One can simply choose to list the genes in descending order indicating the genes with the largest ratio between time points or cell lines to be the most defining for the overall differences in found phenotypes. While this may be accurate to some degree, a more systematic approach that gives a larger overview of all genes and their interactions can be obtained by the Ingenuity Pathway Analysis (IPA, Ingenuity Systems, www.ingenuity.com) which is a commercial licensed product that can display biological function and networks of the analysed genes.

Even though some prefer to analyse data in separate batches of up- and down-regulated genes, the most correct way is to take all genes with altered expression between two treatments or cell lines and analyse the data together. The reason for this is that genes expression may be affected by both inhibitors and activators. A good example would be the Mdm2-p53-Bax interaction. While p53 itself is continuously expressed it is under control from Mdm2 and an increase in Mdm2 levels would hinder p53 activating expression of Bax. So Mdm2 levels goes up and Bax levels goes down but the overall process is downregulation of apoptosis normally induce by p53. If up- and downregulated genes are not included in the same analysis the IPA could assign erroneous pathways and biological processes for the analysed set of genes. On the other hand, inclusion of both up- and downregulated genes in the analysis does give extra work as the networks assigned have to be verified by hand to see if an indicated gene is having the knock-on effect that it should have.

Animal models

The xenograft experiments were conducted with homozygotic nude female NMRI mice of 10 to 12 weeks of age (Homozygous BomTac:NMRI-*Foxn1*^{nu}, Taconic, Denmark). Upon receiving the animals they were transferred from the transport cages to the cages used in the stable and left for approximately 7 days to acclimatise before submitting to experiments. The mice were inspected daily and had access to free feed and water and were kept in a alternating 12 hour light/12 hour dark cycle and housed in a sterile cage with controlled air influx (Scantainer Denmark) and once weekly the mice were weighed. Xenografts were established in the homozygotic nude female NMRI mice. This was achieved by mixing 5*10^6 cells with 50µL Matrigel (DB Bioscience, Europe) and injecting this mixture subcutaneously on the lower back of the mice, 1cm above the root of the tail. After injection of tumour cells, the mice were inspected daily and weighed weekly. Tumours were measured on a daily basis and volume calculated with the formula height*length*width*π/6. Treatment was preformed when tumours reached a volume of 400mm³. The mice were followed until their xenografts reached a maximum of 1200mm³ or the time interval for the experiment ended, at which time the animals were euthanised. All experiments were conducted in accordance with National and International guidelines and with the Danish Animal Experiments Inspectorate's approval.

Eppendorf oxygen electrode

Mice with xenografts of either 400mm³ or 1200mm³ were selected for intratumoural measurement of oxygen levels with the

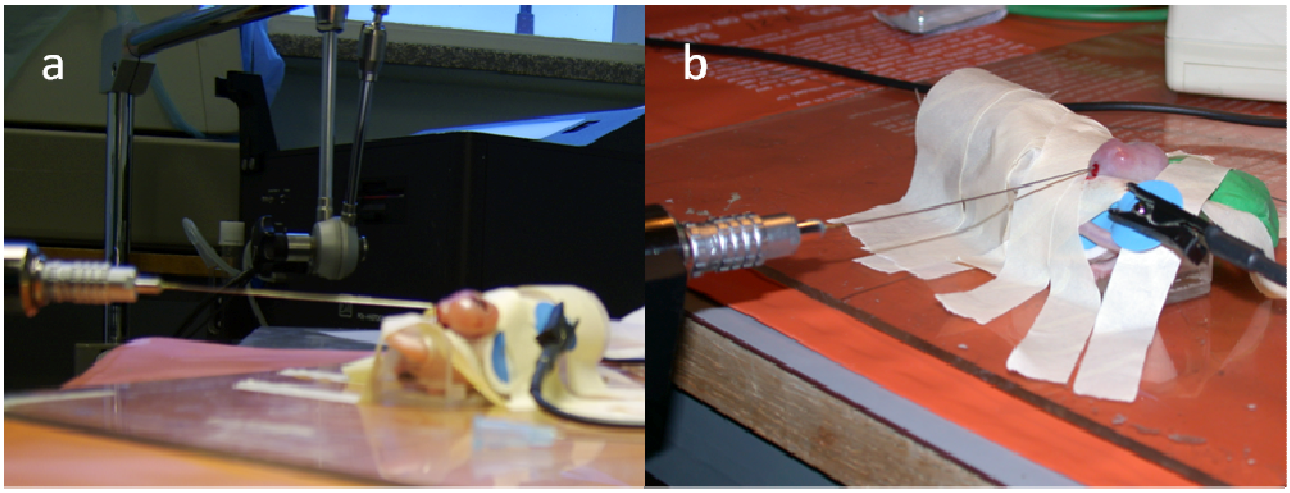

Figure 1 Intratumoural oxygen measurements in xenografts on nude mice.
(a) The Epperdorf histograph is seen in the background. (a,b) The Eppendorf oxygen electrode probe's needle point is entering the xenograft. The blue plate with a wire attached next to the xenograft is the reference electrode. The mouse if fixated in both at plastic rig and ample amounts of tape.

oxygen sensitive needle electrode (KIMOC 5560, pO_2 Histograph, Eppendorf, Germany). Xenografts were subsequently excised for later histopathology and purification of DNA and RNA. Each tumour had a minimum of 5 tracks measured to ensure a representative data collection.

The Eppendorf histograph consists of a needle probe, a reference electrode, and the main component (Figure 1) which both handles data and has a docking station for the needle probe where it can be calibrated. The mechanised needle probe is at the tip only $0.35mm^2$ in diameter and it moves stepwise 0.4 mm forward. The movement is composed of a 0.7mm forward step and then a 0.3mm backwards step to relieve pressure on the electrode membrane.

Due to mechanistic uncertainty of the measured value, then it is feasible to obtain values below 0mmHg, but track containing values below -2.0mmHg were excluded. Tracks with more than one third of its values below 0mmHg were excluded if the other tracks from that tumour were distinctly more oxygenated. Tracks that penetrated through the skin were also discarded, as the track data would contain data points reading the atmosphere. Improper calibration will affect the probe and give false readings, so a standard half an hour calibration was done before usage.

The oxygen electrode data was retrieved from the Eppendorf histograph on venerable floppy disks and reformatted first in Lotus 1-2-3 the subsequent in OpenOfficec 3.0 before final data analysis in State 10 (StataCorp). These steps were necessary due to archaic standards no longer supported by modern spread sheets but which are used to record the data in the Eppendorf Histograph. The collected measurements from all xenografts of the same cell line and size were pooled into one set and subsequently analysed together. From the data set the median, mean, oxygen tension range from the 10^{th} to 90^{th} percentile and the percentage of values below 2.5mmHg, 5mmHg and 10mmHg were calculated. Visualisation of the data was done in SigmaPlot with histograms of the oxygen levels based on all measured xenografts of the same origin and at the same size. Bin size was set to set to 2.5mmHg width and the starting bin is -2.5 to 0mmHg to visualise the lower than 0mmHg values.

All mice were acclimatised in the restraining rig before measurement and handle carefully. A sheet was kept over them to promote a calm response in the animal. If an animal displayed a stressful response during oxygen measurement it was noted in the data journal and the animal was given a short pause before continuing the experiment.

The force of the oxygen electrode is its capability to measure oxygen levels in-situ and its ability to correlate hypoxia with patient outcome. Contrary to histological visualisation of hypoxia, the oxygen electrode measure both acute and chronic hypoxia but also includes necrotic areas. Also there is no oxygen tension limits were is starts registering the hypoxia as with pimonidazole staining were only areas with less than 10mmHg oxygen are visualised. The makes the oxygen electrode a good method for assessing the intratumoural levels of oxygenation and give an estimate of the degree of hypoxia.

Irradiation of nude NMRI mice xenografts

Irradiation of xenografts on the nude mice were done by a 240 kV Philips X-ray machine. The nude mice were restrained in a custom built transparent irradiation jig with room for a maximum of 4 mice, and a custom fitted radiation lead shield for the rig (Figure 2). The restraining and lead shielding ensured that only the tumour received radiation. As the mice were to be kept in sterile environment then the irradiation jig was an airtight construction. To ensure an ample supply of oxygen for the animals a steady stream of air from pressurised flasks were delivered through small filters with 0.2µm pores (Acrodisc Syringe Filters, Pall

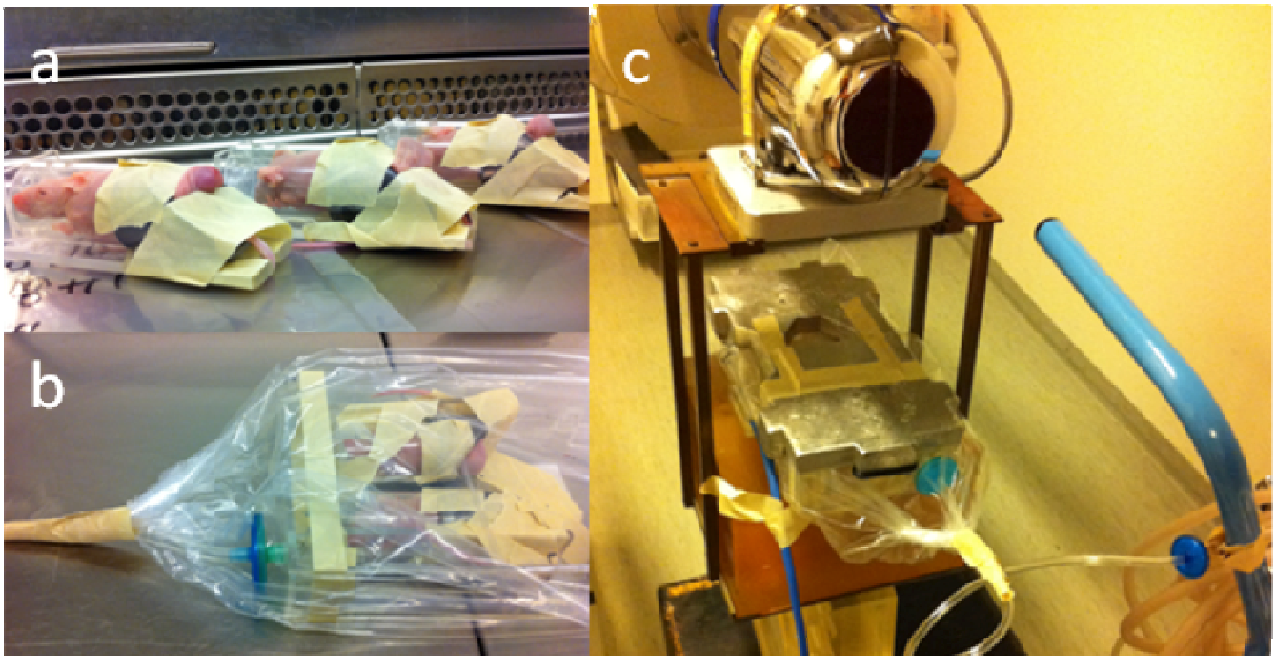

Figure 2 Xenograft bearing nude mice fixated in rigs.
The rigs are cut to fit with the radiation shield so only the exposed xenograft receives radiation. (b) Mice placed in the custom build radiation chamber. The box lid is sealed with Vaseline and it is placed in a plastic bag. A pipe supplies air through filters. (c) Radiation box with the shielding under the radiation cannon. On the left is the handlebar of the pressurised air flask.

Newquay, U.K.). Animals were separated into different treatment groups when their tumours reached a volume of 400mm³ and irradiated with either 0 to 15Gy. To ensure a homogenously radiation field on the tumour, the first half of the dose were delivered from one side, then the jig was flipped 180° and the tumour received the last half of the dose. After radiation the xenografts were measured daily.
A complete remission was noted if there was no observable tumour three months after treatment. Failure was scored when tumours reached three times treatment size, which were 1200mm³, before the time limit. Time from treatment to either failure or the time limit was scored and analysed with Stata 10 and plotted as Kaplan Meyer estimates. The numbers of controlled tumours at each dose was scored and plotted. Analysis of the tumour control data was done with proportional statistics on categorical data.

Immunohistology
All xenografts that were measured with the Eppendorf oxygen electrode had Pimonidazole (0.06mg/kg) injected 1.5 hours in advance of the oxygen measurements. Just after oxygen measurements, but before the mice were euthanized, they were injected with Hoechst 33342 (0.015mg/g). The xenograft was excised and split into three parts. Half of the xenograft was formalin fixed and paraffin embedded (FFPE) and one quarter was frozen and the last quarter was saved in RNAlator (Ambion, Applied Biosystem). Sections were cut from the FFPE half of the xenografts and were mounted on slides, deparaffinised by heating at 60°C overnight and then rehydrated by serial passage through an alcohol gradient consisting of several containers. The rehydrated sections were stained with haematoxylin and eosin for 5min each respectively, before thoroughly rinsing in running water. The slides were dried overnight and cover slips were mounted with glycerol bases mounting media (DPX, BDH). Where applicable section was stained with antibodies and counterstained 2min with either haematoxylin or eosin as needed. Antibody standings were done partly by hand partly by staining robot (Autostainer 408, Lab Vision) and sections were automatically scanned at high resolution for further analysis (Nanozoomer, Hamamatsu, Japan). Visualisation of the blood vessels in the xenografts sections was done by staining with CD34 (clone MEC14.7, Biolegend). The stained sections were scored in regard to both hotspots and randomly accessed viewing fields. The section were scanned at 40x resolution and upon finding a vascular hotspot the numbers of blood vessels were counted at 200x resolution in a 10 x 10 grid covering 0.25mm^2 using LaCavalliers princip [72]. Ten random counts were done on each section as well and the average for each section was reported. For each section at least three hotspots were counted and the highest was selected as representative. Five to ten random counts were done in a similar manner on each section and the average for each section was reported. Non-parametrical Kruskall-Wallis and Dunn's tests were used to compare means for the groups due to non-normal distribution.
Visualisation of the degree of chronic hypoxia was done by staining for pimonidazole with a rabbit antibody (kindly provided by Dr J. A. Raleigh). The image file of the scanned slides was segmented into pimonidazole positive areas and total section area for each slide using ImageJ 1.37c (Wayne Rasband, NIH USA, rsb.info.nih.gov/ij).The scanned slides were exported from NDP.view 1.2.25 (ftp://cdiftp.olympusamerica.com/pub/ndp_view_setup.exe) as TIFF files and loaded into ImageJ where the .tif files were converted into 8-bit grayscale pictures (Figure 3). The image was inverted and trimmed for surrounding artefacts. Thereafter the image was saved in three versions named with suffixes "high", "low" and "grayscale". The "high" and "low" was subsequent edited by adjusting the "windows/Levels" properties of "window level" and "window width" to 26 and 2 for the "high" file and 125 and 125 for the "low" file. Both had their area of pixels with values above 0 (white colour) measured by first selecting the whole image by invoking the ctrl+a shortcut and then measured by invoking the ctrl+m shortcut. The resulting file was subsequently copied to a spread sheet, where the percentage of pimonidazole positive area of the whole section area was noted as the scanned slides Hypoxic Area Fraction (HAF). Comparison statistics was done with the non-parametrical Kruskall-Wallis and Dunn's test, due to non-normal distribution. This approach seems similar to other group's methods [73].
Glucose transporter 1 (GLUT-1 clones ab15309, Abcam) staining was done to visualise both the degree of lower chronic hypoxia as well as the degree of glucose dependence. The overall degree of hypoxia and nutrient undersupply influences GLUT-1 staining pattern as a higher degree of glucose dependence and oxygen starvation forces GLUT-1 from a cytoplasmatic location into being membrane bound. This is also influenced by the distance from the vascular network as GLUT-1 staining near vasculature will tend towards a cytoplasmatic staining whereas the further away the more membrane bound [74].

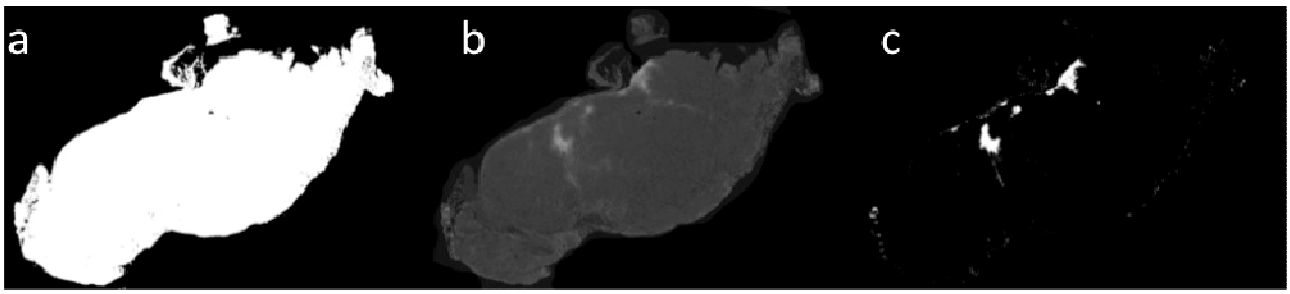

Figure 3 An example of the analysis of pimonidazole positive area.
(b) 8-bit converted grayscale image of the high resolution scanned stained sections. (a) High intensity version of (b) used to obtain the total area of the section. (c) Low intensity version of (b) used to obtain the pimonidazole positive area. The ratio between the pimonidazole positive area over the total section area is noted for each xenograft and the average is scores as the clones Hypoxia Area Fraction. Adapted from manuscript III.

HYPOTHESES

The papers and results presented in this dissertation all aim at investigating the relationship between hypoxia, tumour microenvironment and genetic makeup of cancer stem cell including its tumourigenic potential and how this would affect radiation response. Studies were being done using the hMSC-TERT4, hMSC-TERT20 and clones derived from the latter.

The specific hypotheses of the projects included in this dissertation are as follows:

Carcinogenicity of stem cells

To investigate whether tumourigenicity and radiation resistance is linked, by assessing the genetic alteration and radiation sensitivity between non-tumourigenic and tumourigenic stem cell of the same origin.

Cellular determined radiation resistance

To investigate differences in in-vitro radiation resistance and the genetic profile, phenotypic characteristic and gene expression between tumourigenic cancer stem cell clones, in search for genetic events that may help acquire the trait of radiation resistance.

Microenvironmental or cellular determined radiation resistance in xenografts

To investigate whether the intrinsic cellular radiation resistance (as determined in-vitro) could determine the radiation therapy outcome in murine xenografts taking into account the impact from the microenvironment, hereunder especially hypoxia.

RESULTS

The work presented in this dissertation is from data obtained over the last 4 years. The results obtained are described in details in the three papers included in the appendix of this dissertation. In the following a short summary of the results is presented.

Manuscript I: Tumourigenicity and radiation resistance of mesenchymal stem cells

Analysis with the in-vitro clonogenic surviving fraction assay revealed that the non-tumourigenic stem cell clone TERT4 was more sensitive to radiation treatment and had a lower overall survival than the tumourigenic stem cell clone TERT20 (Figure 4). The non-tumourigenic TERT4 also had a lower PE value than TERT20 (PE=0.292 and 0.395 respectively). The fitted alpha and beta values for the linear-quadratic model gave similar beta values for TERT4 and TERT20 (0.038 and 0.034, respectively), but TERT4 had a larger alpha value than TERT20 (0.59 and 0.42, respectively). TERT4 also had a longer population doubling time than TERT20 (1.3 days for TERT4 and 0.8 days for TERT20).

In-depth analysis using microarray chips revealed a total of 313 genes with different expression levels between control sample of TERT4 and TERT20. A total of 16 genes were found altered between the irradiated samples and the control samples and 6 of these were specifically only expressed in one clone, three for each clone. Several of the genes interacted in networks centred on apoptosis and matrix homeostasis (Table 1). The downregulation of the tumoursuppressor gene PAWR and the upregulation of the genes PLAU and PLAUR, both related to the plasminogen activation system, all affects matrix homeostasis, proliferation and apoptosis induction. This could explain the enhanced survival after radiation treatment. The genes MMP1, MMP14 and TIMP3 are related directly to matrix homeostasis and the altered expression pattern in TERT20 implicating degradation of matrix, which can explain the tumourigenic capability.

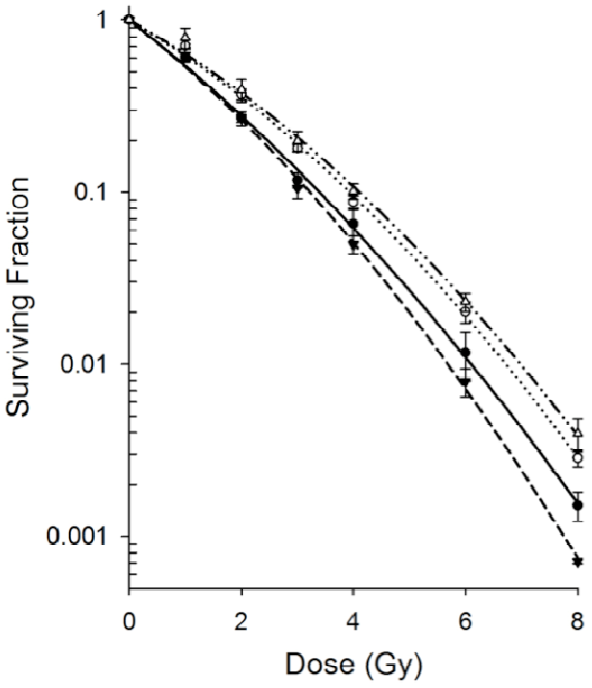

Figure 4 Survival fraction curves for the hMSC-TERT clones.
Cells from the clones were seeded in small flasks at increasing concentration. For each clone, the geometrical mean of 3 SF experiments at each dose level was plotted with one standard error. Overlaid are the linear-quadratic curves based on the alpha and beta values. Adapted from manuscript I and II.

Genes in Ingenuity Networks	Score	Top Functions
Akt, *ASAH1*, ***CEP170***, Collagen Alpha1, *CREG1*, ***DUSP6***, ***EMP1***, ***EREG***, FSH, ***GDF15***, hCG, *IGFBP3*, Lh, LRP, ***MARCH3***, N-cor, *PAWR*, ***PLAU***, ***PLAUR***, *PPAP2A*, *PTPRJ*, SAA, ***SERPINB2***, *SH3BP4*, ***SLC20A1***, *Smad2/3-Smad4*, *SPARC*, ***SPRY2***, ***STC1***, *SULF1*, *TCF4*, *THBS2*, ***TMEM158***, *TPM1*, Vegf	41	Tumor Morphology, Small Molecule Biochemistry, Cell Death
ADAM12, *COL12A1*, *COL1A1*, *COL1A2*, *COL3A1*, *COL4A1*, *COL4A2*, collagen, Collagen type IV, Complement component 1, Creatine Kinase, ***CTSK***, *DCN*, *EFEMP1*, Elastase, *ELN*, *FBLN1*, Fibrinogen, *HSPG2*, *Igfbp*, *IGFBP7*, IL17R, Laminin1, *LOX*, *MFAP5*, ***MMP1***, ***MMP14***, *NID1*, PI3K (complex), *SDC2*, *SERPINH1*, ***SFRP1***, ***SHZB3***, STAT1/3/5 dimer, ***TIMP3***	40	Connective Tissue Disorders, Genetic Disorder, Cellular Assembly and Organization
ANKRD1, *ATP6AP2*, ***CD74***, ***DUSP5***, ***ENPP1***, ***HLA-DMA***, ***HLA-DPA1***, ***HLA-DPB1***, ***HLA-DR***, ***HLA-DRA***, Hla-Drb, ***HLA-DRB1***, ***HLA-DRB5***, ***HMGA2***, *HMGB2*, ***HSP***, IFN Beta, Ifn gamma, IL23, *LGMN*, *LITAF*, MHC, Mhc class ii, MHC Class II (complex), MHC II-β², Mhc2 Alpha, *MYPN*, NFkB (complex), Notch, peptidase, *PLK2*, *TGFB2*, Tlr, *TLR4*, *TXNRD1*	31	Dermatological Diseases and Conditions, Immunological Disease, Inflammatory Disease
Actin, Alpha catenin, ***ARHGDIB***, Cadherin, Caspase, *CDH6*, *CDH11*, ***CDH20***, *CTNND2*, Cyclin A, Cytochrome c, *DOCK5*, *DSP*, E2f, *GOLT1B*, Hdac, *HIST1H3A* (includes others), Hsp27, Hsp70, *HSPA1A*/HSPA1B, Jnk, ***KCNJ2***, MAP2K1/2, ***MAPKAPK3***, MIR1, ***MMD***, *MYBL2*, *NEO1*, ***NETO2***, NfkB1-RelA, ***PREX1***, Pro-inflammatory Cytokine, Rb, Tnf, Tnf receptor	25	Cell Morphology, Cellular Development, Connective Tissue Development and Function
ACTA2, *ACTG2*, *C5orf13*, *CD24*, Collagen type III, Collagen(s), Eotaxin, ERK1/2, ***FERMT2***, Fibrin, G-Actin, Integrin, Integrin alpha 3 beta 1, Integrin alpha 4 beta 1, Integrin alpha 5 beta 1, Integrin alpha 5 beta 3, Integrin alpha V beta 3, Integrinβ², ***ITGA2***, *ITGAV*, ***ITGB3***, *LAMA4*, Laminin, ***LIMA1***, *LPP*, ***LPXN***, ***Metalloprotease***, *MFGE8*, *MYOCD*, *NTN4*, Pdgfr, Smooth Muscle Actin, *TAGLN*, Tenascin, *TNFRSF11B*	24	Cell Death, Hair and Skin Development and Function, Cancer

Table 1 Gene pathways.
Pathway analysis of the altered genes indicates the most likely affected networks in TERT20. Genes with twofold or more upregulation are marked in bold and cursive. Two fold or more downregulation are underscored and cursive. Adapted from manuscript I.

Symbol	Cytoband	Fold	*p*-Value	Response	TaqMan probe ID
Gene with 5-fold or more from expression array					
CTSC	11q14.1	26.4	⩽0.001	Clonal	Hs00175188_m1
GMFG	19q13.2	13.3	⩽0.001	Clonal	Hs00178167_m1
EFEMP1	2p16	12.5	⩽0.001	Clonal	Hs00196287_m1
NNMT	11q23.1	7.4	⩽0.001	Clonal	Hs00244575_m1
CXCL1	4q21	6.3	⩽0.001	Clonal	Hs00236937_m1
CASP1	11q23	3.1	⩽0.001	Clonal	Hs00354836_m1
Genes with 2- to 5-fold from expression array					
BIRC2	11q22	3.1	⩽0.001	Clonal	Hs01112284_m1
PCNA	20p12	1.5	0.0591	Clonal	Hs00427214_g1
CDKN1A	6p21.2	4.0	⩽0.001	Radiation	Hs00355782_m1
MDM2	12q14.3	1.6	0.018	Radiation	Hs00234753_m1
BAX	19q13.3	1.5	0.0196	Radiation	Hs00180269_m1
NAMPT	7q22.3	2.5	n.a	Radiation CE8	Only microarray
Genes with known similar expression					
TERT	5p15.33	1.2	⩾0.1	Expressed	Hs00972656_m1
CD44	11p13	1.2	⩾0.1	Expressed	Hs00153304_m1
CDKN2A	9p21	0.9	⩾0.1	Not expressed	Hs00923894_m1
DBC1	9q32	1.1	⩾0.1	Not expressed	Hs00180893_m1

Table 2 Genes verified by quantitative real time PCR.
Genes from the microarrays found upregulated more that 5-fold or implicated in DNA damage and repair was verified by q-RT-PCR using the listed TaqMAM probes. CD44, CDKN1A, DBC1 and TERT were included, as controls with known similar expression levels. The gene NAMPT showed upregulation after irradiation in CE8 only. The listed fold difference and p-values are from the q-RT-PCR assay. Adapted from manuscript II.

Manuscript II: Cancer Stem Cell overexpression of nicotinamide N-methyltransferase enhances cellular radiation resistance

Close investigation into two tumourigenic stem cell clones derived from TERT20 revealed difference in the in-vitro clonogenic surviving fraction assay after radiation. The clones had similar growth rates in-vitro as both clone used around 0.85 days per population doubling. The PE values of BB3 were higher than CE8 (PE=0.46 and 0.34 respectively, p≤0.05). The clone BB3 was found to be markedly more sensitive to radiation than the clone CE8 (Figure 4). The linear-quadratic model estimated values were different for the alpha value (0.59 and 0.40 for BB3 and CE8 respectively) and for the beta values (0.028 and 0.036, respectively).

Screening for gene differences using micro array chips revealed 53 genes with twofold or more regulation and q-RT-PCR was used to verify several of these. Of the 53 genes 12 were responding to radiation while the rest had a clone specific expression pattern regardless of radiation treatment. Pathway analysis indicated that the genes found with altered gene expression belonged to networks involved in cellular development, growth and proliferation, cell death, DNA replication, DNA repair and cancer. Among the specific genes upregulated in CE8 and which were verified by q-RT-PCR were NNMT and NAMPT (Table 2). Both can influence the energy cycling and the DNA damage repair in the cells as both require nicotinamide as substrate. Nicotinamide is involved in NAD^+ production and inhibition of PARP1 mediated DNA SSB repair. Also the gene PCNA and CASP1 was upregulated in CE8. Both genes encode proteins that regulate the activity of PARP1, as PCNA enhances the rate of activity and Caspase1 degrade the PARP1 protein.

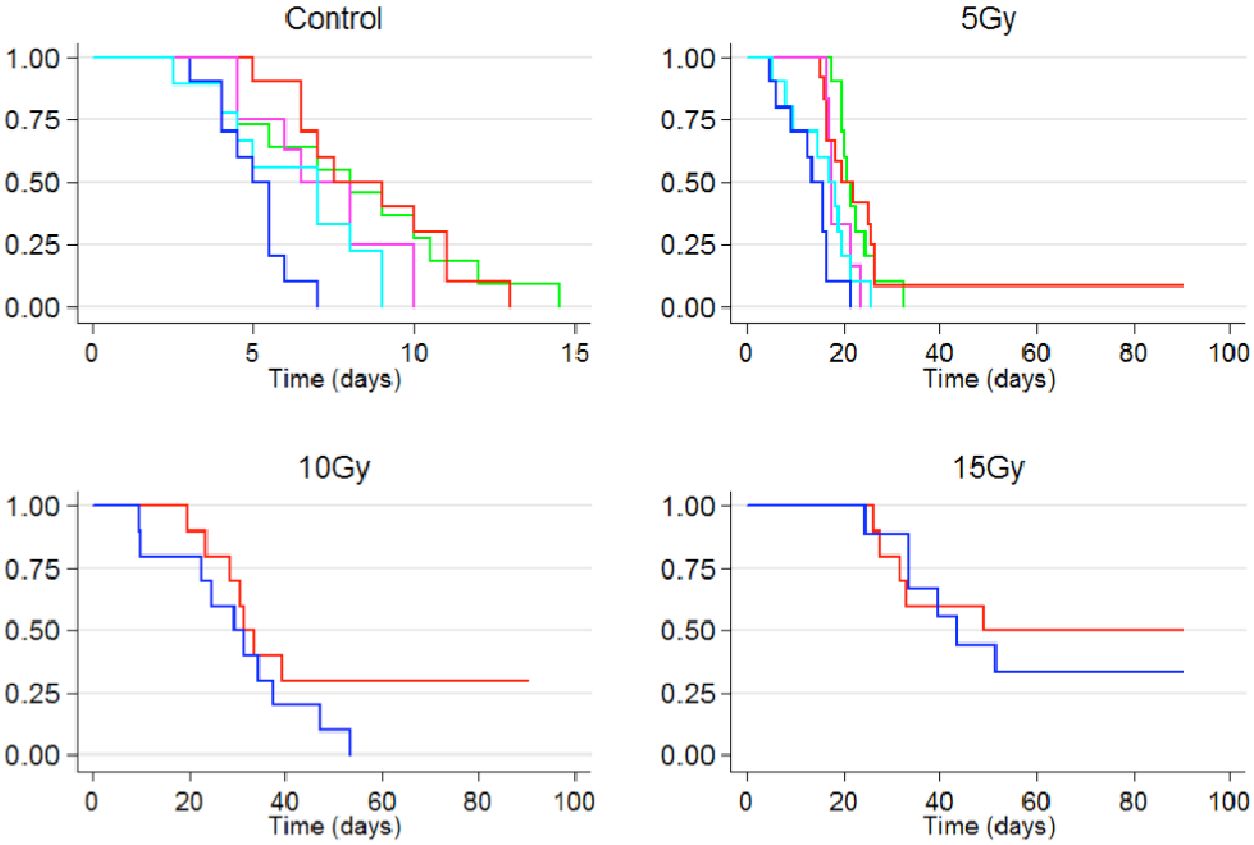

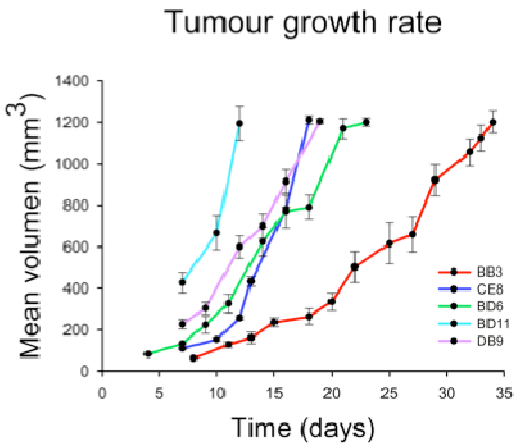

Table III. Degree of tumour control.

	Control	5Gy	10Gy	15Gy
BB3	0 (10)	8 ± 2.3 (12)	30 ± 4.6 (10)	50 ± 5 (10)
CE8	0 (10)	0 (10)	0 (10)	33 ± 5.2 (9)
BD6	0 (11)	0 (10)	n.a.	n.a.
BD11	0 (9)	0 (9)	n.a.	n.a.
DB9	0 (8)	0 (6)	n.a.	n.a.

Percentage of tumours controlled is listed with one standard error and the total numbers of animals per dose group is mentioned in brackets.

Figure 5 Tumour growth and control.
(a) Kaplan-Meyer plots. The growth delay and tumour control as Kaplan Meyer plots for the used treatment doses. Only the time interval from 400mm^3 to 1200mm^3 is estimated over. All clones were assay at 0 (control) and 5Gy, but only BB3 displayed any tumour control. Based on the finding that BB3 is radiation sensitive and CE8 is radiation resistant these two clones were further assay with 10 and 15Gy. (b) Growth curves are plotted median sizes for each clone and the error bars are one standard error. (c) Percentage of tumours controlled is listed with one standard error and the total numbers of animals per dose group are mentioned in brackets. Adapted from manuscript III.

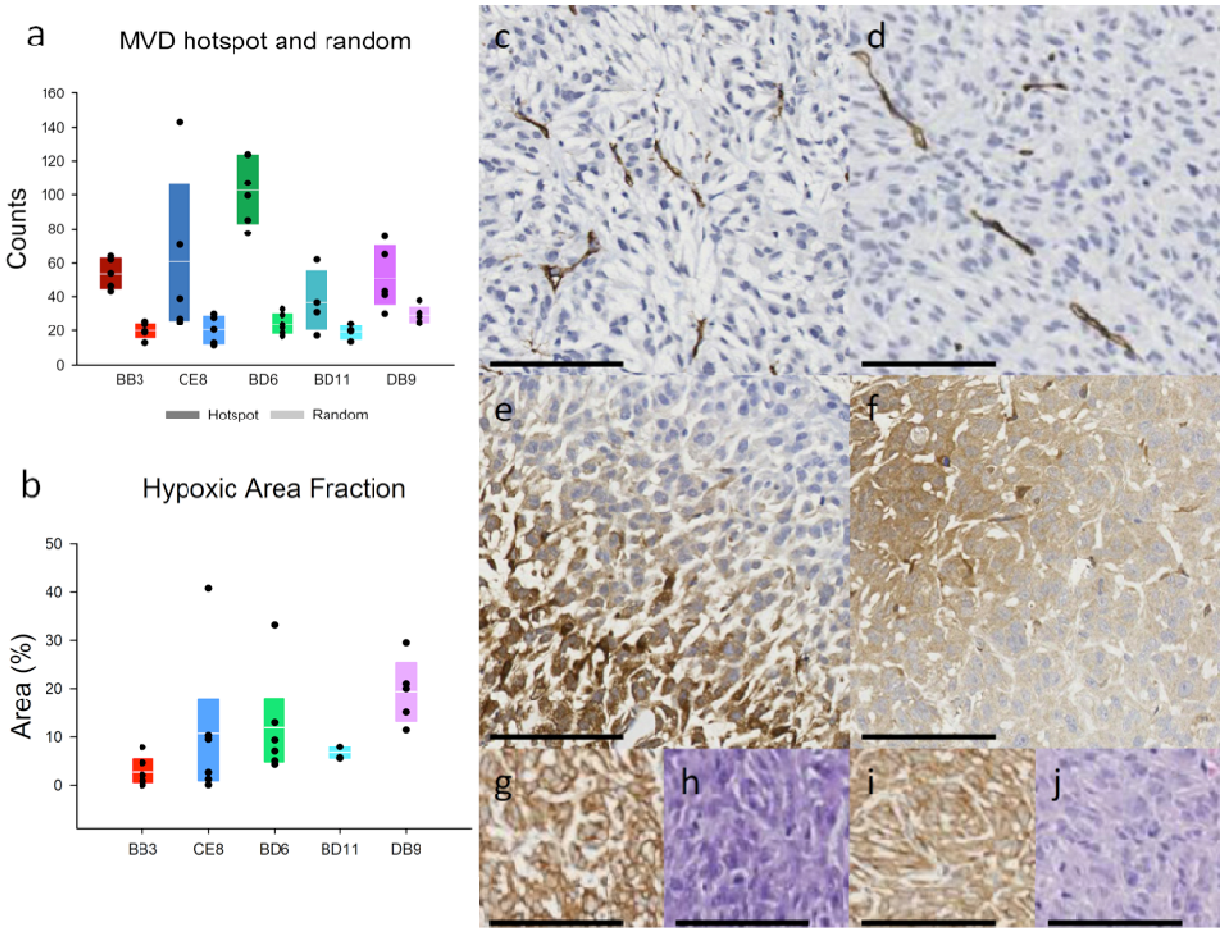

Figure 6 Microenvironmental staining.
(a) Box plot for MVD. Sections stained with anti-murine CD34 antibodies were scanned at 200X resolution for hotspots and counted at 400x resolution. Three selected hotspots and ten random fields were counted three times each for each cell line. Median is indicated by the white bar and the box is defined by the 25 to 75 percentile. The darker coloured box is the hotspot counts and the lighter coloured box is the random counts. (b) Box plot of the HAF for all clones. Section stained with pimonidazole was segmented and analysed in the image analysis program ImageJ and the percentage of the section positive for pimonidazole was plotted for each xenograft at 400mm^3 for each clone. Median is indicated by the white bar and the box is defined by the 25 to 75 percentile. (c-j) Representative stains for anti-CD34 (c,d), pimonidazole (e,f), anti-GLUT1 (g,i) and for haematoxylin and eosin (h,j) are presented for BB3 and CE8 in pairs. The BB3 stains are on the left (c,e,g,h) and the CE8 stains are on the right (d,f,i,j). The black bar on each picture is 100µm. Adapted from manuscript III.

Manuscript III: Tumour microenvironment and radiation response in sarcomas originating from tumourigenic human mesenchymal stem cell

The tumourigenic single cell cloned cell lines from TERT20 consists of not only BB3 and CE8, but also the clones BD6, BD11 and DB9. All clones were capable at generating tumours when implanted as xenografts in immune deficient mice with near similar latency; although BB3 is slower and BD11 is faster than the average in reaching 1200mm^3(Figure 5b). The main differences in growth time were found in the time from injection to the treatment size of 400mm^3. After reaching treatment size the clone had similar growth times. All tested clones exhibit growth delay after irradiation with 5Gy, but the clone BB3 furthermore had tumour control at radiation doses of 5, 10 and 15Gy whereas CE8 only showed limited tumour control at 15Gy (Figure 5c).

When assaying the clones for microenvironmental factors (Figure 6) we found the levels of pimonidazole positive areas to be 1.4% and 6.0% in BB3 and CE8, respectively, but the difference was not statistically significant. Furthermore, the blood vessel per area, as measured by MVD, for both hotspots (median count 54 and 61 for BB3 and CE8 respectively) and random assigned fields (median count 20 for both) revealed no difference between BB3 and CE8. The intratumoural pO_2 Levels, as measured by the Eppendorf Oxygen Electrode, revealed that BB3 had a mean of 4mmHg and 63% of all measurements were below 10mmHg making it the least oxygenated. CE8 had a mean of 13mmHg and only 47% of the measurements were below 10mmHg. This indicated BB3 as being less oxygenated.

The reaming clones displayed levels of SF between BB3 and CE8 and had no tumour control at 5Gy. Their degree of oxygenation at treatment size were also found to be in between BB3 and CE8 with the exception of BD11, that was more oxygenated than the other clones' xenografts. Pimonidazole positive areas showed that only DB9 had a significant higher level than the other clones. The MVD assay indicated that only the BD6 clone differed significantly from the other clones.

CONCLUSIONS

The three manuscripts included in this dissertation reports on the tumourigenicity of mesenchymal cancer stem cells and their intrinsic radiation resistance. The main focus in manuscript I is on the original stem cell lines used as foundation for the cancer stem cell clones describe in manuscript II and III. The discussion regarding manuscript II and III will focus on the clones BB3 and CE8.

Manuscript I: Tumourigenicity and radiation resistance of mesenchymal stem cells

Several steps are to be in place before a tumour can occur. TERT20 and TERT4 both have higher expression of the telomerase subunit TERT which helps them avoid senescence and have bestowed them with longevity [65, 66]. Furthermore, both have no contact inhibition at the population doubling levels used in our experiments and both have a deregulation in the cell cycle through the mutation in the gene CDKN2A [66] and the lack of expressed p16 will allow unchecked progression out of G1 phase [22]. Albeit both display these same phenotypes only TERT20 is tumourigenic.

When looking into the details between TERT20 and TERT4 gene expression using IPA it was found that TERT20, in comparison to TERT4, have a downregulation of the tumoursuppressor gene PAWR, which is involved in the apoptotic pathway [75]. The genes PLAU and PLAUR are involved in several aspects of tumourigenicity as upregulation of the genes are involved in proliferation, apoptosis evasion and matrix degradation [76, 77]. Furthermore several genes only related to matrix homeostasis were found altered in TERT20 so as to promote matrix degradation. The normal inhibition by TIMP3 of the matrix degrading MMP1 and MMP14 [78] is lacking and MMP1 activity has been linked with tumour invasion and metastasis [79, 80].

The altered gene expression pattern together with the indicated biological functions of cancer, cell death and matrix development, as indicated by IPA tools underscores that TERT20 is a tumourigenic cell line. The deregulation of genes involved in apoptosis could be the main reason behind the found difference in radiation resistance. Furthermore TERT20 also seems capable of regulating the surrounding matrix and thereby facilitating tumour invasion, and perhaps even evade apoptosis to a degree and that gives TERT20 the advantage over the non-tumourigenic TERT4 cell line. This falls in line with the observation that TERT20 is tumourigenic when injecting into immune deficient animals [66, 70]. As no single specific cause seems to fully explain the difference in radiation resistance, then several of the found elements may have to be present for the TERT20 cancer stem cell line to be able to evade apoptosis. Possible candidates are genes like PLAU and PLAUR which seem to promote both apoptosis evasion and tumour invasion. Overall we find that the mesenchymal CSC are more radiation resistant than mesenchymal stem cells of the same origin.

Manuscript II: Cancer Stem Cell overexpression of nicotinamide N-methyltransferase enhances cellular radiation resistance

The tumourigenic subclones from TERT20 were not selected for any capabilities other that being capable of surviving the single cell cloning [70]. The inherited trait of tumourigenicity from the TERT20 was retained in all clones, but the enhanced radiation resistance was not passed on to all subclones. The clone BB3 exhibited radiation resistance similar to TERT4 and the clone CE8 had similar resistance as TERT20 (Figure 4). The two subclones had similar population doubling times so the difference in surviving fraction after irradiation had to originate from their genetic background.

Investigations into the differences between the subclones revealed several genes with altered expression levels. Of particular interest were the genes NNMT and NAMPT which both were upregulated in CE8 and both encode for enzymes that require nicotinamide as a substrate (Figure 7) [81]. NNMT uses nicotinamide as a substrate to mark unwanted compounds in the cell for excretion [82] and NAMPT used nicotinamide as a precursor that is turned it into NAD^+. Both genes therefore influence the energy cycling in the cell either by limiting or by promoting NAD^+ generation. The presence of nicotinamide in the cell is critical for the repair of single strand breaks as the protein PARP1 requires NAD^+ [25], but at the same time PARP1 activity is also inhibited by high levels at nicotinamide [81].

The main driving factor behind the difference in NNMT levels between the clones could be the lack of one of chromosome 11 in CE8, where NNMT gene is located. As the analysis for chromosomal integrity was done with TERT20 as common reference then we know that BB3 and TERT20 have both chromosomes 11 intact. The clone differs in radiation resistance even though they originate from the same cell line and this has not been selected for. It is plausible that, because of its continuous passaging, then the

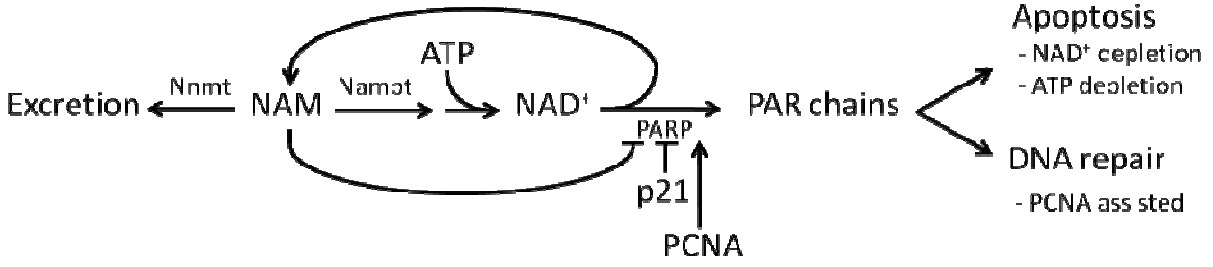

Figure 7 Nicotinamide cycle.

PARP activity is both depended upon and inhibited by nicotinamide (NAM). Nicotinamide is converted into NAD+ by several steps, including Nampt, and NAD+ is used as cofactor in the polymerisation of PAR chains at the site of SSB. PARP uses NAD+ and releases nicotinamide. The PAR chain recruits DNA repair complexes. PCNA increases DNA polymerase efficiency and is reported to interact with PARP; therefore PCNA could also have an impact on the repair rate. Nicotinamide is methylated by Nnmt and thereafter excreted, thus reducing the freely available nicotinamide for NAD+ synthesis. PARP activity reduces the intra cellular levels of both ATP and NAD+. A lack of both can induce apoptosis. PARP is negatively regulated by p21 and negatively feedback inhibited by nicotinamide levels.

TERT20 cell line has become a conglomerate of several slightly divergent subclones, and that the single cell cloning simply has highlighted this.

Manuscript III: Tumour microenvironment and radiation response in sarcomas originating from tumourigenic human mesenchymal stem cell

The TERT20 cell line is tumourigenic and so are its subcloned cell lines BB3, CE8, BD6, BD11 and DB9 [70]. The sixth subclone BC8 also display tumourigenicity but at a much lower degree of success and therefore it was excluded from further experiments. The remaining cell lines displayed, at the tumour size of 400mm^3, nearly similar patterns for the chronic hypoxia marker pimonidazole and MVD assayed with CD34. The only exception were DB9 which seemed more chronically hypoxic than the rest of the clones and BD6 which had a much higher score for the CD34 assayed MVD when counting the hotspot. The intratumoural oxygen levels, as measured by the Eppendorf Oxygen Electrode, display some dissimilarity between the clones. BB3 was found to be the most hypoxic of the clones, CE8 and DB11 was the best oxygenated clone and BD6 and DB9 lay as intermediates between BB3 and the well oxygenated.

The only clone which exhibited a degree of control already at 5Gy was BB3. Upon expanding the dose levels for BB3 and CE8 the difference were found to be more marked as CE8 only display control at 15Gy whereas BB3 had a higher degree of control with increasing dose.

Overall, Xenografts from the clone BB3 seemed slightly more hypoxic than xenografts from CE8, although there were no difference in MVD and HAF. Even with this slight difference in the microenvironmental factor with most impact for radiotherapy outcome, BB3 was still more radiation sensitive. This is in line with the result obtained in manuscript II where BB3 was found to be more radiation sensitive in-vitro than CE8 and proves that in-vitro radiation resistance can predict the radiation therapy outcome of xenografts when microenvironmental factor are not different.

FUTURE PERSPECTIVES

Protein level verification

The most critical work that remains to be done is protein level verification of several of the implicated markers and proteins. The $CD44^+CD24^-$ cellular marker difference between TERT4 and TERT20 and its subclones, should preferably be verified on tumour sections but will also need to be done on cell suspension using flow cytometry in the case of the non-tumourigenic TERT4. Tumour pieces that are homogenised to single cells could also be analysed for the $CD44^+CD24^-$ marker by flowcytometry, but caution is needed as the process is known to strip cells of surface markers.

The protein levels of NNMT and NAMPT genes in BB3 and CE8 tumour sections and cell samples need to be verified. In tumours this if preferably done by immunohistochemistry. Alternatively, assayed by screening in-vitro cell samples by western blotting, and there include TERT4, TERT20 and the rest of the subclones.

Model verification

When implementing the hMSC-TERT models we simply adopted the previous use of the clones without assessing the lowest number of cells needed for successful xenograft take. From working with a murine leukaemia cell line in our labs it is known that as little as 100 cells can successfully induce the same outcome as 100,000 cells, albeit with a longer time before visible symptoms. In that context 5,000,000 cells per injection seems a little over dimensioned. On the other hand, the original papers published on the hMSC-TERT20 clones used the high number of cells per injection and a deviation form that number would hinder the direct comparison between previous results and new results. One factor that would definitely change is the time to treatment size, as fewer cells would need longer time before reaching the number of cell needed for that size.

Functionalistic verification

Further investigations into the functionality of NNMT, nicotinamide and DNA damage repair could be conducted by knocking down the NNMT expression in the radiation resistant clone by siRNA and then submitting it to the in-vitro surviving fraction assay. A lowered surviving fraction would prove a link between the observed radiation resistance and the increased expression of NNMT. This concept could also be used in-vivo with the tumour control assay. Alternatively, NNMT overexpression could be introduced via homolog recombination or retroviral insertion, into the radiation sensitive clone in an attempt to gain a more radiation resistant phenotype.

There are several genes listed in manuscript I that could base the foundation of functionalistic assays into the cause of tumourigenicity of either the original TERT20 cell line or it subclones. The gene PAWR is a prominent target as it is tumoursuppressor found downregulated in TERT20. Knocking the PAWR gene out in TERT4 and subsequent submitting it to xenograft experiments would reveal whether this gene is singular responsible for the tumourigenic phenotype

Also PLAU and PLAUR downregulation in TERT20 is an interesting experiment as these genes may affect the TERT20 ability to evade apoptosis. Using the SF assay with TERT20 clones where either genes are siRNA downregulated would reveal if there is any substance in the apoptosis evasion implicated.

The genes found in TERT20 that affects the degradation of the intracellular matrix could be reinstated into a normal level of expression, by either up- or downregulation, to see if the hindrance to the intercellular matrix homeostasis is a significant contributor to the TERT20 tumourigenic capabilities, and therefore its subclones tumourigenitic capabilities. It would be interesting to upregulate LOX and TIMP3, by homolog recombination or retroviral insertion, or knockdown of the TIMP3 targets MMP1 or MMP14, with siRNA, to see if the altered matrix homeostasis is important for the tumourigenic capability in-vivo.

One curious experiment that could be conducted is the radiation resistant enhancement of the radiation sensitive clone BB3 through serial selection of the surviving colonies after multiple rounds of radiation treatment. The radiation selection would likely give rise to a more radiation resistant subclone of BB3 that could be compared to the original radiation sensitive BB3 clone revealing alternative routes to radiation resistance.

Since TERT20 and CE8 both are CSC, then their stemness could be the main culprit for the enhanced radiation resistance observed. Applying forced differentiation of the CSC may alter the outcome for the surviving fraction assay and the xenograft experiments. Forced differentiation could be attempted either mechanistically, as by culturing the cell on morphological structures promoting differentiation [83], systematically, as by hyperthermia [84--86], or chemically, as by culturing the clones with bone promoting factors in a similar setup as used for the original non-

tumourigenic hMSC-TERT2 [65] or through cell differentiation regulation by using kinase inhibitors [87].

SUMMARY

Cancer stem cells are emerging as a new critical target for successful outcome in radiation treatment, as prognosis for patients with stem cell positive tumours are worse than average. The majority of the cells composing the tumour burden may be killed off by the radiation doses normally used in standard treatment, but the cancer stem cells may escape cell death due to their heightened damage resistance. Whereas the influence of hypoxic areas on radiation therapy is well described and countered by selective extra treatment when needed, there is currently no specific treatment against cancer stem cells. Therefore, understanding the fundamental mechanisms of cancer stem cells' resistance to treatment and their response to radiotherapy is of interest.

Several cell lines derived from a unique human mesenchymal cancer stem cell model, consisting of both a non-tumourigenic and several tumourigenic stem cell lines, were used to investigate the relationship between tumourigenicity, radiation resistance and stemness of cancer cells.

Using the non-tumourigenic and tumourigenic clones the relationship between tumourigenicity and radiation resistance of stem cells were investigated. The cancer stem cells were more radiation resistant than normal stem cells and this could be due to the described difference in gene expression. Several genes involved in matrix maintenance and apoptosis had altered levels of expression and this could be the driving force behind the cancer stem cells enhanced radiation resistance.

Difference in in-vitro radiation resistance was found between two closely related tumourigenic clones. The enhanced radiation resistance seems to stem from the overexpression on the NNMT gene. This gene is linked with resistance to both chemotherapy and radiation and encodes an enzyme, which consumes nicotinamide. The DNA single strand repair protein PARP1 is inhibited by nicotinamide and lower cellular levels may enhance DNA damage repair, thereby granting radiation resistance.

The observed in-vitro radiation resistance was found to predict in-vivo radiation resistance of the same clones as measured by tumour control. The xenografts were found to have no difference in microenvironmental factors, hereunder especially hypoxia. This corroborates the genetic cause for radiation resistance.

Overall the results indicate a link between tumourigenicity and radiation resistance for cancer stem cells. These results support the cancer stem cell theory and furthermore underscore the need for targeting cancer stem cell in the clinic.

REFERENCE LIST

1. Turesson I. The progression rate of late radiation effects in normal tissue and its impact on dose-response relationships. Radiotherapy and Oncology 1989;15:217-26.
2. Rodemann HP, Bamberg M. Cellular basis of radiation-induced fibrosis. Radiotherapy and Oncology 1995;35:83-90.
3. Shafiq J, Barton M, Noble D, Lemer C, Donaldson LJ. An international review of patient safety measures in radiotherapy practice. Radiother Oncol 2009;92:15-21.
4. Korreman S, Rasch C, McNair H et al. The European Society of Therapeutic Radiology and Oncology-European Institute of Radiotherapy (ESTRO-EIR) report on 3D CT-based in-room image guidance systems: A practical and technical review and guide. Radiotherapy and Oncology 2010;94:129-44.
5. Wouters BG, Begg AC. Irradiation-induced damage and the DNA damage reaponse. In: Joiner M, van der Kogel A, editors. Basic Clinical Radiobiology. 4th Edition. London: Hodder Arnold, 2011;11-26.
6. Dantzer F, de Murcia G, Ménissier-de Murcia J, Nasheuer HP, Vonesch JL. Functional association of poly(ADP-ribose) polymerase with DNA polymerase α-primase complex: A link between DNA strand break detection and DNA replication. Nucleic Acids Res 1998;26:1891-8.
7. Xu Y, Baltimore D. Dual roles of ATM in the cellular response to radiation and in cell growth control. Genes & Development 1996;10:2401-10.
8. Stiff T, O'Driscoll M, Rief N, Iwabuchi K, Löbrich M, Jeggo PA. ATM and DNA-PK Function Redundantly to Phosphorylate H2AX after Exposure to Ionizing Radiation. Cancer Res 2004;64:2390-6.
9. Toshiyuki M, Reed JC. Tumor suppressor p53 is a direct transcriptional activator of the human bax gene. Cell 1995;80:293-9.
10. Chipuk JE, Kuwana T, Bouchier-Hayes L et al. Direct Activation of Bax by p53 Mediates Mitochondrial Membrane Permeabilization and Apoptosis. Science 2004;303:1010-4.
11. Wade Harper J, Adami GR, Wei N, Keyomarsi K, Elledge SJ. The p21 Cdk-interacting protein Cip1 is a potent inhibitor of G1 cyclin-dependent kinases. Cell 1993;75:805-16.
12. Branzei D, Foiani M. Regulation of DNA repair throughout the cell cycle. Nat Rev Mol Cell Biol 2008;9:297-308.
13. Rassool FV, Gaymes TJ, Omidvar N et al. Reactive Oxygen Species, DNA Damage, and Error-Prone Repair: A Model for Genomic Instability with Progression in Myeloid Leukemia? Cancer Res 2007;67:8762-71.
14. Kinsella TJ. Coordination of DNA Mismatch Repair and Base Excision Repair Processing of Chemotherapy and Radiation Damage for Targeting Resistant Cancers. Clin Cancer Res 2009;15:1853-9.
15. Ikejima M, Noguchi S, Yamashita R et al. The zinc fingers of human poly(ADP-ribose) polymerase are differentially required for the recognition of DNA breaks and nicks and the consequent enzyme activation. Other structures recognize intact DNA. J Biol Chem 1990;265:21907-13.
16. Herceg Z, Wang ZQ. Functions of poly(ADP-ribose) polymerase (PARP) in DNA repair, genomic integrity and cell death. Mutat Res 2001;477:97-110.
17. Li X, Heyer WD. Homologous recombination in DNA repair and DNA damage tolerance. Cell Res 2008;18:99-113.
18. Mladenov E, Iliakis G. Induction and repair of DNA double strand breaks: The increasing spectrum of non-homologous end joining pathways. Mutation Research/Fundamental and Molecular Mechanisms of Mutagenesis 2011;711:61-72.
19. Kastan MB, Onyekwere O, Sidransky D, Vogelstein B, Craig RW. Participation of p53 Protein in the Cellular Response to DNA Damage. Cancer Res 1991;51:6304-11.
20. Shieh SY, Ikeda M, Taya Y, Prives C. DNA Damage-Induced Phosphorylation of p53 Alleviates Inhibition by MDM2. Cell 1997;91:325-34.
21. Barak Y, Juven T, Haffner R, Oren M. mdm2 expression is induced by wild type p53 activity. EMBO 1993;12:461-8.
22. Ouelle DE, Zindy F, Ashmun RA, Sherr CJ. Alternative reading frames of the INK4a tumor suppressor gene

encode two unrelated proteins capable of inducing cell cycle arrest. Cell 1995;83:993-1000.
23. Zhang Y, Xiong Y. Mutations in Human ARF Exon 2 Disrupt Its Nucleolar Localization and Impair Its Ability to Block Nuclear Export of MDM2 and p53. Molecular Cell 1999;3:579-91.
24. Herceg Z, Wang ZQ. Failure of Poly(ADP-Ribose) Polymerase Cleavage by Caspases Leads to Induction of Necrosis and Enhanced Apoptosis. Mol Cell Biol 1999;19:5124-33.
25. Ha HC, Snyder SH. Poly(ADP-ribose) polymerase is a mediator of necrotic cell death by ATP depletion. Proceedings of the National Academy of Sciences 1999;96:13978-82.
26. Berger NA. Poly(ADP-Ribose) in the Cellular Response to DNA Damage. Radiat Res 1985;101:4-15.
27. Earnshaw WC. Apoptosis: lessons from in vitro systems. Trends in Cell Biology 1995;5:217-20.
28. Reya T, Clevers H. Wnt signalling in stem cells and cancer. Nature 2005;434:843-50.
29. Shay JW, Wright WE. Telomeres and telomerase in normal and cancer stem cells. FEBS Letters 2010;584:3819-25.
30. Bianco P, Riminucci M, Gronthos S, Robey PG. Bone Marrow Stromal Stem Cells: Nature, Biology, and Potential Applications. Stem Cells 2001;19:180-92.
31. Chamberlain G, Fox J, Ashton B, Middleton J. Concise Review: Mesenchymal Stem Cells: Their Phenotype, Differentiation Capacity, Immunological Features, and Potential for Homing. Stem Cells 2007;25:2739-49.
32. Vogelstein B, Kinzler KW. Cancer genes and the pathways they control. Nat Med 2004;10:789-99.
33. Reya T, Morrison SJ, Clarke MF, Weissman IL. Stem cells, cancer, and cancer stem cells. Nature 2001;414:105-11.
34. Bao S, Wu Q, McLendon RE et al. Glioma stem cells promote radioresistance by preferential activation of the DNA damage response. Nature 2006;444:756-60.
35. Baba T, Convery PA, Matsumura N et al. Epigenetic regulation of CD133 and tumorigenicity of CD133+ ovarian cancer cells. Oncogene 2008;28:209-18.
36. Suvà ML, Riggi N, Stehle JC et al. Identification of Cancer Stem Cells in Ewing's Sarcoma. Cancer Res 2009;69:1776-81.
37. Terry J, Nielsen T. Expression of CD133 in Synovial Sarcoma. Applied Immunohistochemistry & Molecular Morphology 2010;18
38. Al-Hajj M, Wicha MS, Benito-Hernandez A, Morrison SJ, Clarke MF. Prospective identification of tumorigenic breast cancer cells. Proceedings of the National Academy of Sciences 2003;100:3983-8.
39. Dittfeld C, Dietrich A, Peickert S et al. CD133 expression is not selective for tumor-initiating or radioresistant cell populations in the CRC cell lines HCT-116. Radiother Oncol 2009;92:353-61.
40. Strauss R, Li Z-Y, Liu Y et al. Analysis of Epithelial and Mesenchymal Markers in Ovarian Cancer Reveals Phenotypic Heterogeneity and Plasticity. PLoS ONE 2011;6
41. Buess M, Rajski M, Vogel-Durrer BM, Hermann R, Rochlitz C. Tumor-Endothelial Interaction Links the $CD44^{+}/CD24^{-}$ Phenotype with Poor Prognosis in Early-Stage Breast Cancer. Neoplasia 2009;11:987-1002.
42. Charafe-Jauffret E, Ginestier C, Iovino F et al. Breast Cancer Cell Lines Contain Functional Cancer Stem Cells with Metastatic Capacity and a Distinct Molecular Signature. Cancer Res 2009;69:1302-13.
43. Zeppernick F, Ahmadi R, Campos B et al. Stem Cell Marker CD133 Affects Clinical Outcome in Glioma Patients. Clin Cancer Res 2008;14:123-9.
44. Eramo A, Lotti F, Sette G et al. Identification and expansion of the tumorigenic lung cancer stem cell population. Cell Death Differ 2007;15:504-14.
45. Hanahan D, Weinberg RA. The Hallmarks of Cancer Review. Cell 2000;100:57-70.
46. Bernhard EJ. Interventions that induce modifications in the tumor microenvironment. Cancer/Radiothérapie 2011;15:376-82
47. Hall EJ, Bedford JS, Oliver R. Extreme Hypoxia; its Effect on the Survival of Mammalian Cells Irradiated at High and Low Dose-rates. Br J Radiol 1966;39:302-7.
48. Gray LH, Conger AD, Ebert M, Hornsey S, Scott OCA. The Concentration of Oxygen Dissolved in Tissues at the Time of Irradiation as a Factor in Radiotherapy. Br J Radiol 1953;26:638-48.
49. Nordsmark M, Alsner J, Keller J et al. Hypoxia in human soft tissue sarcomas: Adverse impact on survival and no association with p53 mutations. Br J Cancer 2001;84:1070-5.
50. Diehn M, Cho RW, Lobo NA et al. Association of reactive oxygen species levels and radioresistance in cancer stem cells. Nature 2009;458:780-3.
51. Horsman MR. Measurement of tumor oxygenation. International Journal of Radiation Oncology*Biology*Physics 1998;42:701-4.
52. Vaupel P. Tumor microenvironmental physiology and its implications for radiation oncology. Seminars in Radiation Oncology 2004;14:198-206.
53. Kopp HG, Avecilla ST, Hooper AT, Rafii S. The Bone Marrow Vascular Niche: Home of HSC Differentiation and Mobilization. Physiology 2005;20:349-56.
54. Calabrese C, Poppleton H, Kocak M et al. A Perivascular Niche for Brain Tumor Stem Cells. Cancer Cell 2007;11:69-82.
55. Keith B, Simon MC. Hypoxia-Inducible Factors, Stem Cells, and Cancer. Cell 2007;129:465-72.
56. McCord AM, Jamal M, Williams ES, Camphausen K, Tofilon PJ. CD133+ Glioblastoma Stem-like Cells are Radiosensitive with a Defective DNA Damage Response Compared with Established Cell Lines. Clin Cancer Res 2009;15:5145-53.
57. Jamal M, Rath BH, Williams ES, Camphausen K, Tofilon PJ. Microenvironmental Regulation of Glioblastoma Radioresponse. Clin Cancer Res 2010;16:6049-59.
58. Yu J, Vodyanik MA, Smuga-Otto K et al. Induced Pluripotent Stem Cell Lines Derived from Human Somatic Cells. Science 2007;318:1917-20.
59. Takahashi K, Tanabe K, Ohnuki M et al. Induction of Pluripotent Stem Cells from Adult Human Fibroblasts by Defined Factors. Cell 2007;131:861-72.
60. Zhou H, Wu S, Joo JY et al. Generation of Induced Pluripotent Stem Cells Using Recombinant Proteins. Cell Stem Cell 2009;4:381-4.
61. Covello KL, Kehler J, Yu H et al. HIF-2α regulates Oct-4: effects of hypoxia on stem cell function, embryonic development, and tumor growth. Genes & Development 2006;20:557-70.

62. Gordan JD, Bertout JA, Hu CJ, Diehl JA, Simon MC. HIF-2α Promotes Hypoxic Cell Proliferation by Enhancing c-Myc Transcriptional Activity. Cancer Cell 2007;11:335-47.
63. Taub R, Kirsch I, Morton C et al. Translocation of the c-myc gene into the immunoglobulin heavy chain locus in human Burkitt lymphoma and murine plasmacytoma cells. Proceedings of the National Academy of Sciences 1982;79:7837-41.
64. Bodnar AG, Ouellette M, Frolkis M et al. Extension of Life-Span by Introduction of Telomerase into Normal Human Cells. Science 1998;279:349-52.
65. Simonsen JL, Rosada C, Serakinci N et al. Telomerase expression extends the proliferative life-span and maintains the osteogenic potential of human bone marrow stromal cells. Nat Biotechnol 2002;20:592-6.
66. Serakinci N, Guldberg P, Burns JS et al. Adult human mesenchymal stem cell as a target for neoplastic transformation. Oncogene 2004;23:5095-8.
67. Abdallah BM, Haack-Sørensen M, Burns JS et al. Maintenance of differentiation potential of human bone marrow mesenchymal stem cells immortalized by human telomerase reverse transcriptase gene despite [corrected] extensive proliferation. Biochem Biophys Res Commun 2005;326:527-38.
68. Burns JS, Abdallah BM, Shrøder HD, Kassem M. The histopathology of a human mesenchymal stem cell experimental tumor model: support for an hMSC origin for Ewing's sarcoma? Histol Histopathol 2008;23:1229-40.
69. Grønbæk K, Ralfkiaer U, Dahl C et al. Frequent hypermethylation of DBC1 in malignant lymphoproliferative neoplasms. Mod Pathol 2008;21:632-8.
70. Burns JS, Abdallah BM, Guldberg P, Rygaard J, Schroder HD, Kassem M. Tumorigenic Heterogeneity in Cancer Stem Cells Evolved from Long-term Cultures of Telomerase-Immortalized Human Mesenchymal Stem Cells. Cancer Res 2005;65:3126-35.
71. Larsen KH, Frederiksen CM, Burns JS, Abdallah BM, Kassem M. Identifying a molecular phenotype for bone marrow stromal cells with in vivo bone-forming capacity. J Bone Miner Res 2010;25:796-808.
72. Offersen BV, Borre M, Overgaard J. Quantification of angiogenesis as a prognostic marker in human carcinomas: a critical evaluation of histopathological methods for estimation of vascular density. European Journal of Cancer 2003;39:881-90.
73. Zips D, Le K, Yaromina A et al. Triple angiokinase inhibition, tumour hypoxia and radiation response of FaDu human squamous cell carcinomas. Radiother Oncol 2009;92:405-10.
74. Airley R, Loncaster J, Davidson S et al. Glucose transporter glut-1 expression correlates with tumor hypoxia and predicts metastasis-free survival in advanced carcinoma of the cervix. Clin Cancer Res 2001;7:928.
75. El-Guendy N, Zhao Y, Gurumurthy S, Burikhanov R, Rangnekar VM. Identification of a Unique Core Domain of Par-4 Sufficient for Selective Apoptosis Induction in Cancer Cells. Mol Cell Biol 2003;23:5516-25.
76. Sidenius N, Blasi F. The urokinase plasminogen activator system in cancer: Recent advances and implication for prognosis and therapy. Cancer Metastasis Rev 2003;22:205-22.
77. Gondi CS, Kandhukuri N, Dinh DH, Gujrati M, Rao JS. Downregulation of uPAR and uPA activates caspase mediated apoptosis, inhibits the PI3k/AKT pathway. Int J Oncol 2007;31:19.
78. Sternlicht MD, Werb Z. How matrix metalloproteinases regulate cell behavior. Annu Rev Cell Dev Biol 2001;17:463.
79. Hotary KB, Allen ED, Brooks PC, Datta NS, Long MW, Weiss SJ. Membrane Type I Matrix Metalloproteinase Usurps Tumor Growth Control Imposed by the Three-Dimensional Extracellular Matrix. Cell 2003;114:33-45.
80. Boire A, Covic L, Agarwal A, Jacques S, Sherifi S, Kuliopulos A. PAR1 Is a Matrix Metalloprotease-1 Receptor that Promotes Invasion and Tumorigenesis of Breast Cancer Cells. Cell 2005;120:303-13.
81. Sauve AA. NAD+ and Vitamin B3: From Metabolism to Therapies. J Pharmacol Exp Ther 2008;324:883-93.
82. Kim J, Hong S, Lim E et al. Expression of nicotinamide N-methyltransferase in hepatocellular carcinoma is associated with poor prognosis. J Exp Clin Cancer Res 2009;28:20.
83. Dalby MJ, Gadegaard N, Tare R et al. The control of human mesenchymal cell differentiation using nanoscale symmetry and disorder. Nature materials 2007;6:997-1003.
84. Trieb K, Sztankay A, Amberger A, Lechner H, Grubeck-Loebenstein B. Hyperthermia inhibits proliferation and stimulates the expression of differentiation markers in cultured thyroid carcinoma cells. Cancer Letters 1994;87:65-71.
85. Sharif-Khatibi L, Kariminia A, Khoei S, Goliaei B. Hyperthermia induces differentiation without apoptosis in permissive temperatures in human erythroleukaemia cells. Int J Hyperthermia 2007;23:645-55.
86. Nørgaard R, Kassem M, Rattan SIS. Heat Shock-Induced Enhancement of Osteoblastic Differentiation of hTERT-Immortalized Mesenchymal Stem Cells. Ann NY Acad Sci 2006;1067:443-7.
87. Dancey J, Sausville EA. Issues and progress with protein kinase inhibitors for cancer treatment. Nat Rev Drug Discov 2003;2:296-313.